Flat plate boundary layer accelerated by shock wave propagation

Florian Hermet, Nicolas Binder, Jérémie Gressier

Flat plate boundary layer accelerated by shock wave propagation

Florian Hermet[1], Nicolas Binder[1], Jérémie Gressier[1]

[1]ISAE-SUPAERO, Université de Toulouse, France

(Received xx; revised xx; accepted xx)

The flat plate transitional boundary layer response to the acceleration induced by the shock wave propagation is studied using large-eddy simulations (LES). The steady boundary layer global behaviour is firstly investigated before focusing on the transient response of a turbulent region following the shock wave propagation. It is shown that the transient response of the turbulent region exhibits strong similarities with the spatial transition process to turbulence induced by free-stream turbulence, the so-called bypass transition. The boundary layer does not evolve gradually from the initial turbulence intensity to the final one but undergoes a temporal transition process composed of three distinct phases. These three different phases are comparable with the three stages of a bypass transition (i.e. *buffeted laminar flow*, *transition* and *fully turbulent*) since there are governed by the same physical processes. On the other hand, it is highlighted that this temporal response is identical to that described by He & Seddighi (2013) during the study of an incompressible boundary layer undergoing an increase of mass flow rate. The boundary layer compression by the shock propagation does not contribute to any significant change in the turbulence dynamic after an unsteady acceleration.

Key words: Boundary layer, shock wave propagation, temporal transition process

1. Introduction

1.1. *Motivation and scope*

The interaction of a shock wave with a boundary layer is a flow configuration frequently addressed in the open literature. Not only for own academic sake, aiming at the comprehension of mechanisms related to non-equilibrium turbulence (see Jamme et al. 2002; Larsson & Lele 2009), but also for engineering purposes. Aeronautics provides many application cases, such as super-critical wings (Lee 2001) or transonic/supersonic air intakes (Babinsky & Harvey 2011). But in most situations, the shock position is stationary or oscillating around a given position. Recent trends in propulsion are looking toward the feasibility of Pulsating Detonating Engines (Heiser & Pratt 2002). In such engines, shock waves propagate through the rear part of the engine, including the turbine stages. Those turbine stages experience the lowest Reynolds numbers in the engine (Mayle 1991), together with a strong turbulence intensity produced in the combustion chamber. The transition issues thus become an additional challenge for both the design of the blades and the flow simulation. This offers a new situation where a propagating unsteady shock wave periodically interacts with a transitional boundary layer developed at the wall of complex geometries. Surprisingly, the corresponding canonical configuration, a high Reynolds number compressible flow over a flat plate submitted to the transient passage

of a shock wave, has been very scarcely examined so far. One of the few corresponding references is that of He & Seddighi (2013) which depicts the temporal response of a turbulent boundary layer following an increase in mass flow rate in an incompressible flow. The flow temporal response to the transient regime was found similar to the spatial transition process to turbulence induced by free-stream turbulence, the so-called bypass transition.

However, such a mechanism has never been analyzed in compressible flows. The present contribution is intended to fill this gap. A brief summary of previously published work on both dynamic acceleration of boundary layers and bypass transition is now proposed. Then the numerical approach is presented in a second part and the initial state of the boundary layer is described in a third one. The boundary layer's dynamic response to the shock's passage is then detailed in the last part of the paper before concluding this work.

1.2. *Temporal acceleration of turbulent flow*

The seminal questioning regarding the turbulence dynamic response to a transient flow can be credited to Maruyama et al. (1976), who experimentally examined the influence of a sudden increase or decrease of water mass flow on the turbulence structure. An ingenious valve system allowed them to double or half the mass flow rate in the test channel within very short time scales (0.05s to 0.5s). The wall shear stress and the axial velocity of the flow were quantified using an electrochemical method. In this paper, the first denomination of the initial turbulent state is found, which is named *old* turbulence. The article describes how the final state is either an evolution of the *old* turbulence, such as is the gradual decay observed for a brutal deceleration, or the possible emergence of a brand new structuring, called *new* turbulence, as observed for an acceleration.

A detailed investigation of transient incompressible flow in a pipe was carried out by He & Jackson (2000), using water as the working fluid. Linear increase or decrease of the turbulent Reynolds ($Re_\tau = \frac{u_\tau \delta}{\nu}$) were investigated between an initial steady-state and a final steady-state. The mean velocity, the root-mean-square velocity and the turbulent shear stress were measured during the acceleration thanks to a three-beam, two-component laser Doppler anemometer. This research has prevailed as the first detailed study of ramp-type transient turbulent flow. This article revealed some striking features of the turbulence response of a transient flow to the community. He & Jackson (2000) identified three distinct delays in turbulence response, during an increase of turbulent Reynolds number. These different delays are respectively associated to: (i) the characteristic time of the turbulence production response, (ii) the characteristic time for the turbulent energy redistribution and (iii) delay associated with the turbulence diffusion within the boundary layer. These successive responses of the turbulence have also been observed numerically. Jung & Chung (2012) carried out large-eddy simulations of the linear temporal acceleration of an incompressible turbulent boundary layer whose results are in agreement with the turbulence response mechanism proposed by He & Jackson (2000).

More recently, He & Seddighi (2013) proposed another interpretation, based on direct numerical simulations of an incompressible turbulent boundary layer subjected to a mass flow rate increase. It seems that the turbulence dynamics during the transient phase follows a transition process comparable to that of a bypass transition that would develop spatially on a flat plate. The flow evolves from the *old* turbulence to the *new* turbulence through three successive phases (*pre-transition*, *transition*, and *fully turbulent*) which are similar to the three distinct regions characterizing a bypass-transition process in a transitional boundary layer. The paper details the exact mechanism, which can be

summarized as follows: the brutal mass-flow increase induces high strain rates localized near the wall. This thin layer then spreads into the boundary layer. The interaction of this additional shear stress with the pre-existing turbulence is the root of a *new* turbulent state: the *old* turbulence thus plays the role of free-stream turbulence in the usual spatial bypass transition. During the *pre-transition*, the boundary layer undergoes a receptivity process: the *old* turbulence is modulated to generate elongated streaks of high and low streamwise velocities that remain stable at this step. During the *transition* phase, these streaks degenerate into turbulent spots that grow and merge. Then the regime becomes *fully turbulent*, after having contaminated with the *new* turbulence properties the whole of the boundary layer thickness. He & Seddighi (2015) have examined the influence of the final-to-initial Reynolds number ratio on the temporal transition mechanism. When this ratio is low† ($Re_1/Re_0 < 1.5$), the streaks no longer seem to be identifiable in the boundary layer. However, an analysis of the fluctuations reveals that the boundary layer still undergoes a laminar-turbulent transition process.

Similar findings were reported in Jung & Kim (2017) where direct numerical simulations allow determining more precisely the influence of Re_1/Re_0. The temporal transition mechanism and its different steps have also been confirmed experimentally by Mathur et al. (2018), which has investigated transient flows caused by an incompressible acceleration in the range $Re_1/Re_0 \in [2; 10]$, thanks to PIV measures.

The bypass transition is thus a reference on which the temporal transition mechanism is assessed. We now propose a brief focus on this mechanism and highlight the associated pieces of knowledge useful to keep in mind for the present study.

1.3. *Bypass transition*

The transition to turbulence was first observed by Reynolds (1883). Since this seminal work, it is now common knowledge that the Reynolds number governs the transition from a laminar to a turbulent state. However, this transition does not occur for a universal Reynolds number. This critical value highly depends on environmental disturbances which can have many sources: free-stream turbulence, surface default, acoustic waves, etc. The boundary layer response to external disturbances gives rise to different boundary layer transition processes. For low environmental disturbances, the transition process is governed by the slow amplification of two-dimensional waves, known as T-S waves. When the environmental disturbances are more intense, typically Tu $> 1\%$, the T-S waves are completely overshadowed by the transient growth phenomenon. The disturbances amplification and their breakdown are then more rapid. Elongated streaks of high and low streamwise velocities appear in the transitional boundary layer. This transition process is the so-called bypass transition.

Bypass transition has a spatial evolution which can be divided into three regions: the *buffeted laminar boundary layer*, an *intermittent* region and the *fully turbulent* boundary layer. In the initial stage of bypass transition, the free-stream disturbances penetrate the laminar boundary layer, which has its own *receptivity*. This process is dictated by the *shear sheltering* mechanism (Jacobs & Durbin 1998). The boundary layer acts as a low-pass filter. The shear layer filters out high-frequency disturbances from the external flow and allows low-frequency disturbances to penetrate. In this first region, disturbances are amplified to generate elongated streaks of high and low streamwise velocities, so-called *Klebanoff mode* (Klebanoff 1971; Kendall 1985). The *lift-up* effect, introduced by Landahl (1980), is now considered by the active community of bypass transition to be the mechanism behind these streaks. Streaks are caused by a modulation of the

† In He & Seddighi (2013), $Re_1/Re_0 = 2.64$.

streamwise momentum cause by the normal fluctuations of the wall. Also, during the streaks growth, Kendall (1985) experimentally observed the evolution of the streamwise velocity fluctuations (square root averaged) inside the boundary layer. This profile reaches a maximum, which can be scaled with $\sqrt{x}$. A theoretical justification for such scaling is proposed by Andersson et al. (1999) and Luchini (2000), thanks to an analysis of the energy growth rate, using the optimal disturbances theory. Moreover, Luchini (2000) argued that during the streaks growth, the streamwise RMS velocity profile is scaled by y/δ_u, and with this normalization $u'_{rms,max}$ is located at a $y/\delta_u = 1.33$. These last two properties, as well as the streaks presence, have been widely accepted by the community as distinctive features of the first region of a bypass transition, and can be used as such to assess the nature of the transitional process. Such objective criteria allowed an investigation of the critical Reynolds number. Fransson et al. (2005) investigated experimentally the influence of Tu and found that the critical Reynolds number is proportional to Tu^{-2}. Streamwise velocity perturbations are amplified up to about $0.1U_e$ before the first turbulent spots are observed (Matsubara & Alfredsson 2001). This reports the beginning of the second stage: the *intermittent* region. The streaks breakdown were mainly observed thanks to direct numerical simulations (Jacobs & Durbin 2001; Hack & Zaki 2014). Only two main breakdown mechanisms seem to appear (Brandt et al. 2004) depending on the perturbation environmental nature: the sinuous and the varicose breakdowns (see Schlatter et al. (2008) for more details on streaks breakdown). During the *intermittent* region, the turbulent spots grow until they completely fill the boundary layer thickness, which marks the last stage: the boundary layer becomes *fully turbulent*.

The numerical method used to assess the similarity between a spatial bypass transition and the transient process provoked by a shock wave passage is now detailed.

2. Methodology

2.1. *Flow solver*

The present large-eddy simulations are performed using an in-house solver, so-called IC^3 forked from $\mathrm{CharLES}^{\mathrm{X}}$ solver (Brès et al. 2017), which solves the spatially filtered compressible Navier-Stokes equations in their conservative form using a finite volume formulation on unstructured meshes. An explicit third-order Runge-Kutta scheme is used for time advancement, while a solution-adaptative methodology, which combines a non-dissipative centered numerical scheme and an essentially non-oscillatory (ENO) second-order shock-capturing scheme, is used to compute flux. The ENO scheme is applied in regions around shock waves, identified by a shock sensor based on local dilatation, enstrophy and sound speed (Bermejo-Moreno et al. 2014). Unresolved effects of small-scale fluid motions are represented thanks to the Vreman subgrid-scale model (Vreman 2004), which is particularly suited for transitional flow.

2.2. *Numerical configuration*

The computational domain used for numerical simulations is represented on figure 1. A turbulent injection condition is used as inlet boundary condition, see Klein et al. (2003). This boundary condition is based on the *digital filtering* approach and requires an adaptation distance allowing the turbulence statistics to reach the proper characteristics. Consequently, half of the flat plate length (also called chord) ($30\delta_{bdf,i}$) is prescribed between the inlet condition and the flat plate leading-edge. This corresponds to a greater length than that recommended by Touber & Sandham (2009) to reach the proper characteristics ($20\delta_{bdf,i}$) with this boundary condition.

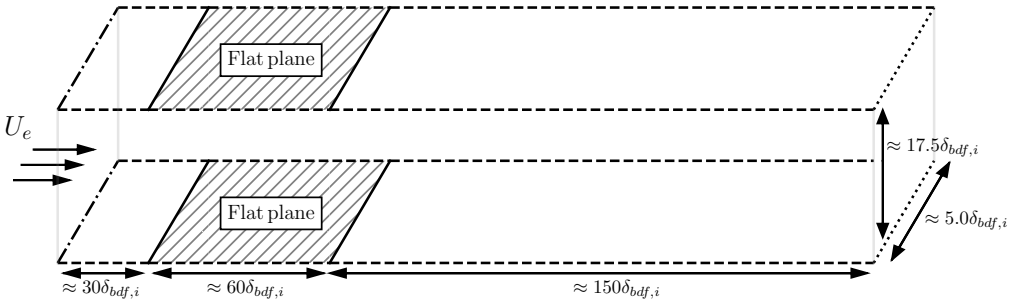

Figure 1: Computational domain.

Isotropic turbulence with Tu = 5% is prescribed by the inlet boundary condition during the initial steady regime, see the table 1. Such a large setting, representative of gas turbine applications, also promotes a bypass transition of the boundary layer.

The shock wave is generated by an average flow discontinuity suddenly imposed at the inlet condition. The shock wave intensity was chosen moderate $P_1/P_0 = 1.5$, table 1, so that Mach number downstream the shock remains subsonic.

The characteristics of the post-shock turbulence are not known *a priori*. This is a difficulty since those characteristics are prescribed in the inlet condition. An extensive preliminary analysis would be required to adapt the turbulence inlet condition to the mean flow. The turbulence rate at the inlet was kept constant throughout the simulation to limit calculation costs. The turbulence rate injected is therefore different from that naturally prescribed by the shock propagation. This inadequate inflow condition contaminates the simulation and moves with the flow velocity. Thus, the shock has to interact with the flat plate boundary layer, and the local turbulence must find its own final equilibrium before the inadequate inflow turbulence reaches the leading edge (see figure 2). The long-distance which has been set at the upstream of the flat plate (initially required by the evolution of synthetic turbulence into isotropic turbulence) and the low Mach number of the final state ensure that such a condition is verified.

Also, the pressure outlet condition was pushed out further from the plate trailing edge to avoid any shock wave reflection, which could disturb the region of interest. On the lateral boundaries, periodicity conditions are used to make the ensemble averages convergence less costly. This distance between the periodic boundaries is part of the following discussion.

2.3. *Transient flow analysis*

Due to the mean flow unsteadiness, ensemble averages cannot be computed using temporal averages. Five repetitions of the simulation are performed to complete ensemble averages. The initial condition for each repetition is set at different times of the same steady-state initial regime. Approximately one advection time (> 20 times the integral time scale) on the plate separates each of the simulations to ensure the turbulence temporal decorrelation between them. In addition to these simulations, the configuration was chosen to solve two independent flat plate boundary layers in one run. Also, due to the periodic boundaries, the flow is homogeneous in spanwise direction. The results average in spanwise direction is fundamental to approach a strict convergence of the ensemble averages.

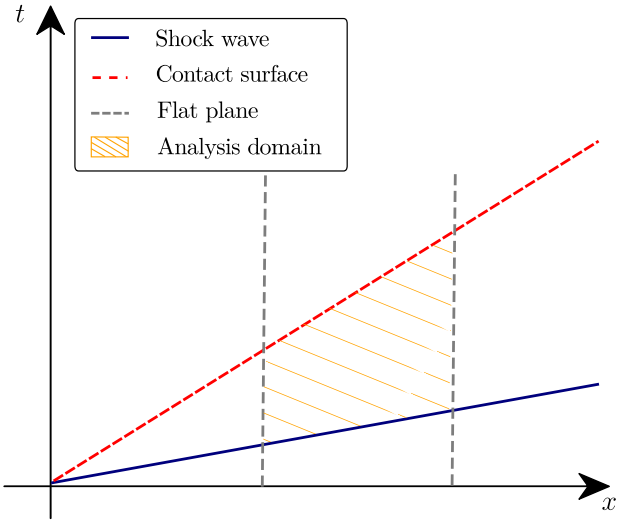

Figure 2: Transient flow analysis region.

2.4. *Numerical methodology validation*

Based on the channel height, the Reynolds number (Re_D) increases suddenly downstream of the shock wave. The final flow thus requires a more constraining mesh than the initial flow. Consequently, at identical mesh, the initial flow resolution is finer than the final flow. However, due to a wider boundary layer thickness, the initial flow requires a larger domain to ensure the correlation approaches zero within the half-width of the domain and thus guaranty that the periodicities on the lateral boundaries do not constrain the turbulence.

	$\mathrm{Re_D}$	Mach	$\mathrm{Tu_{inlet}}$	$P_{\mathrm{inlet}}/P_{\mathrm{outlet}}$	Δx^+	Δy^+	Δz^+	Mesh size
Initial flow	2.3×10^5	0.15	5%	1.00	20	0.4	12	110M
Final flow	9.0×10^5	0.40	–	1.50	60	1.2	36	110M

Table 1: Flow and mesh parameters of the present study.

The mesh is validated by checking the turbulent boundary layer for the initial and final states†, compared with DNS turbulent boundary layer data computed by Schlatter & Örlü (2010). The boundary layer thickness increases along the plate, the mesh is only validated for a chosen abscissa, located at 70% of the chord, corresponding at $Re_{\theta,initial,70\%} = 1210$ and $Re_{\theta,final,70\%} = 2500$. Details of the mesh used in the present study is given in table 1.

The mean velocity profiles of the initial and final flow are very well predicted with the adopted mesh, figure 3. The linear law and the logarithmic region show excellent agreement with the reference data (Schlatter & Örlü 2010). The logarithmic region is larger for the final flow due to an increase in Re_θ. Concerning Reynolds stresses, some differences appear between the present study and the reference data. In the boundary layer outer region, Reynolds stresses differ since the turbulence rate in the external flow differs between the various simulations. For the initial flow, Reynolds stresses are well

† The final state is found when mean quantities are steady.

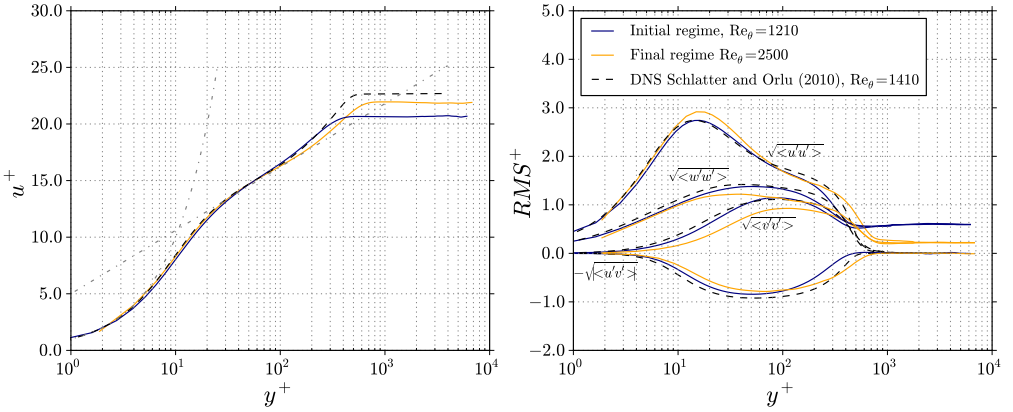

Figure 3: Simulations comparison of steady boundary layer at 70% of chord with DNS of Schlatter & Örlü (2010).

captured in the inner region of the boundary layer. For the final flow, the resolution of Reynolds stress is less accurate, due to a lower mesh resolution. However, the Reynolds stress variations are correctly returned so that the mesh resolution is judged suitable.

Usual LES mesh recommendations are based upon past experience regarding boundary layers with turbulence in equilibrium. In transient flow, additional checks are required. Two-points correlation is often used to ensure the computational domain relevance during the transient regime (He & Seddighi 2013). Streamwise velocity correlation in the transverse direction ($R_{11,z}$) is evaluated throughout the transient regime (see figure 4) to verify that the lateral periodicity does not constrain the turbulence. Figure 4 shows a $R_{11,z}$ representation during the transient regime at 99% of the chord for $y^+(t) = 200$ since this is one of the most critical abscissas. Before the shock propagation, $t^* < 0$, the correlation pattern is constant since the boundary layer is at equilibrium, with a negative value region due to the flow homogeneity in the transverse direction. For initial flow, the domain width is very well adapted since correlation approaches zero within the half-width of the domain. During the shock propagation $t^* = 0$, the correlations are modified. Small oscillations are visible, revealing a slight lack of convergence. However, it is important to note that, during the transient regime, the correlation reaches a value close to zero over a shorter distance than that required for the initial flow ($t^* < 0$). Therefore, the domain width is sufficient to allow turbulence development in the spanwise direction during the transient regime.

3. Initial boundary layer description

An instantaneous visualization of the boundary layer is given in the figure 5 (upper part). Iso-surfaces of low and high streamwise fluctuation velocities are shown above the wall to illustrate the transition process. At the same time, the free-stream turbulence is presented on the normal cut plane. Elongated streaks of positive and negative streamwise velocity fluctuations are found (around $Re_\theta = 200$). This region corresponds to the *buffeted laminar boundary layer* described by Jacobs & Durbin (1998). At $Re_\theta = 280$, streaks growth leads to turbulent spots that still coexist with other streaks: this is the beginning of the *transition* stage. This stage ends approximately at $Re_\theta = 600$ when the turbulence completely contaminates the boundary layer thickness. These steps of the transition process are also noticeable on the spatial evolution of the friction coefficient,

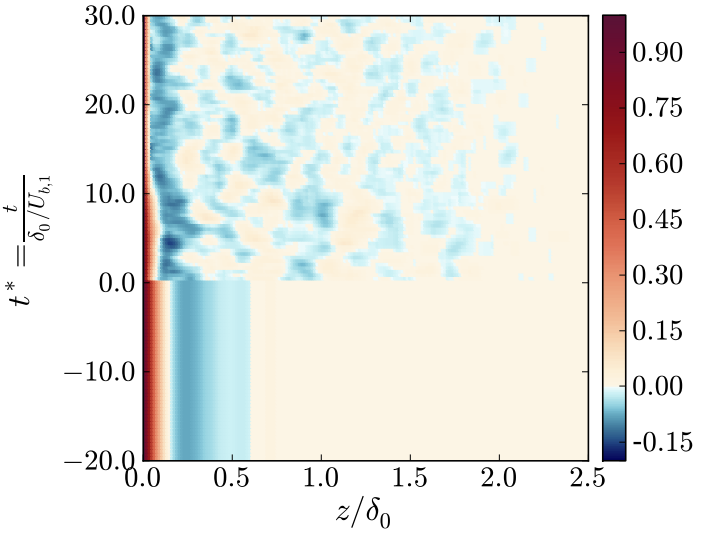

Figure 4: Unsteady visualisation of the streamwise velocity correlation in the transverse direction, at 99% of the chord for $y^+(t) = 200$.

figure 5 (lower part). Initially, the boundary layer is *laminar* and follows the Blasius theoretical prediction, see Schlichting & Gersten (2017). When streaks appear in the boundary layer, the friction coefficient slightly deviates from the Blasius prediction: the laminar boundary layer is *buffeted*. The *transition* region is the stage for which the growth of the friction coefficient happens since turbulent spots promote mixing. After this stage, the boundary layer is fully *turbulent*, and the friction coefficient gets in steady decreasing, in accordance with the thickening of the boundary layer. The friction coefficient of the turbulent region shows excellent agreement with the turbulent correlation from Cebeci & Cousteix (2005), displaying that the near-wall resolution of the initial flow is good. The free-stream turbulence level and the presence of elongated streaks strongly suggest that a bypass transition is obtained. However, confirmation is sought through the analysis of fluctuations, as aforementioned in the introduction.

The left plot of the figure 6 depicts the maximum disturbances along the plate. After a delay, which can be interpreted as the *receptivity* process of the boundary layer to external perturbations, turbulent kinetic energy has a linear increase before reaching a saturation threshold and then decreases. This behaviour is typical of a bypass process, according to Matsubara & Alfredsson (2001). The disturbances amplification begins when the streamwise elongated streaks are generated. Consequently, only the streamwise component of the fluctuating motion is affected. Spanwise and normal components are modified when turbulent spots appear in the boundary layer, which marks the second stage of the process: the transition region. This is associated with the growth of the pressure-strain correlation term, which reorders the turbulent kinetic energy between the components of fluctuating motion. Anyway, the maximum of $u'_{rms,max}$ continues to grow in the rear part of this second stage despite the activation of the mechanism of redistribution of the turbulent kinetic energy. In that region, the boundary layer structure is still dominated by elongated streaks, which extract energy from the mean flow at a greater rate than it is redistributed. The gradual growth of the turbulent spots to the detriment of streaks modifies this energy cascade, and $u'_{rms,max}$ finally reaches a maximum and then decays.

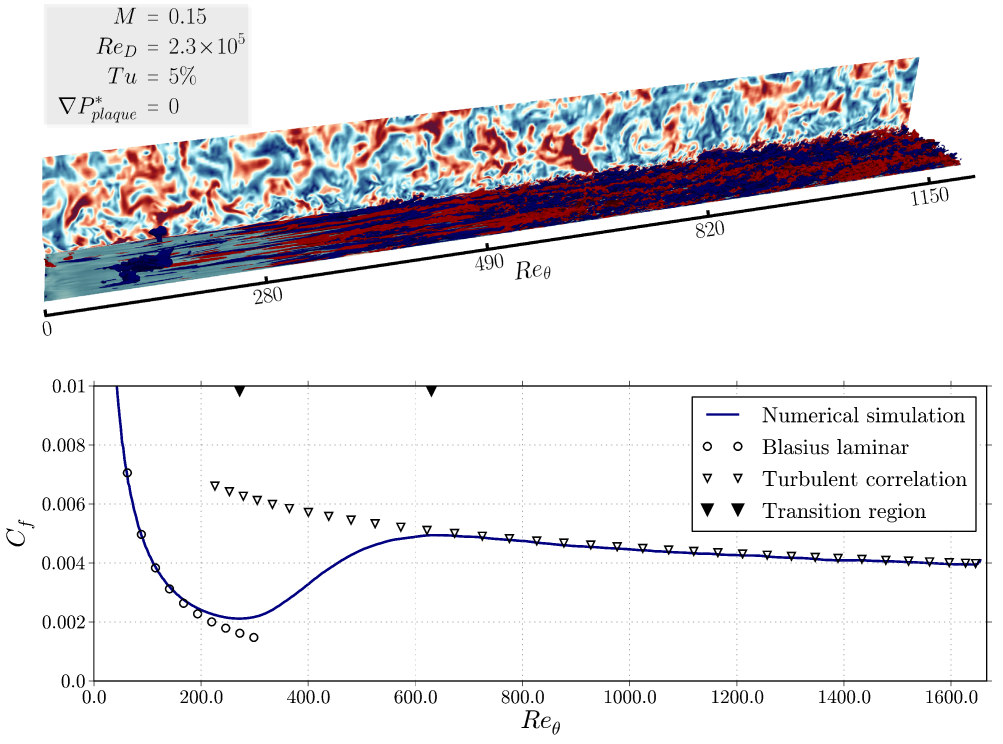

Figure 5: Top: Above the wall: iso-surfaces of high (red) and low (blue) streamwise velocity fluctuations corresponding respectively to $-0.08U_e$ and $0.08U_e$. Orthogonal to the wall: Free-stream turbulence. Below: Friction coefficient. $Re_\theta \in [180; 280]$: *buffeted laminar boundary layer*; $Re_\theta \in [280; 600]$: *transition*; $Re_\theta > 600$: *fully turbulent*.

The right plot of the figure 6 confirms that $u'_{rms}/u'_{rms,max}$ profiles are scaled in y/δ_u during the linear amplification process, with a maximum located at $y/\delta_u \approx 1.33$, as depicted by Luchini (2000) for a bypass process.

Those results demonstrate that the numerical method is adequate and that the setting is adapted to the generation of a bypass transitional boundary layer as an initial state for the transient flow. This boundary layer is now accelerated by a shock wave (table 1), and the associated results are presented in the next section.

4. Results and discussion

4.1. *General behaviour of the transient boundary layer*

The figure 7 gives the spatial evolution of the friction coefficient at different times during the transient regime while the figure 8 illustrates the instantaneous flow for the same time. The shock propagation induces a large increase of the friction coefficient, very clear at instants (b) and (c), which was also noticed by He & Seddighi (2013) during the acceleration of an incompressible boundary layer. The shock wave brutally accelerates the flow all in one piece, including the entire boundary layer and the closest positions near the wall, as will be demonstrated in the next section. This is the origin of the sudden

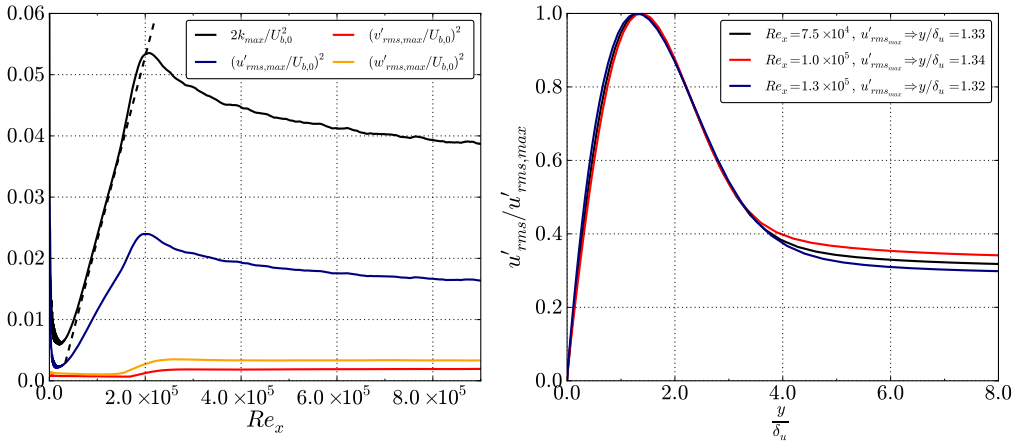

Figure 6: Left: disturbances maximum along the plate. Right: $u'_{rms}/u'_{rms,max}$ profile for several Re_x. $U_{b,0}$ correspond to the boundary layer external velocity of the initial flow.

rise of wall shear stress. Then, a large decrease in the friction coefficient is observed, for example at instants (b), (c), and (d). The flow seems to reach a *quasi-laminar* regime, confirmed by the extinction of the fluctuations downstream of the wave, observed on the figure 8. A temporal acceleration tends to relaminarize the boundary layer, in the same way a spatial acceleration does. We will see later that this can be explained by the slow response of Reynolds stresses compared with the modification of the mean flow which occurs instantaneously when the shock propagates. The end of the transient phase is marked by the progressive evolution of the boundary layer to a new state of equilibrium, as seen at instants (d), (e) and (f).

In the final steady-state, the location of the transition has been pushed downstream. This can be explained by the reduction of Tu, figure 8, compared with the initial state. The decreases of turbulence intensity, downstream of the shock wave, is the result of the stabilising effect of acceleration on the turbulence, see Sreenivasan (1982). Since the transition abscissa is inversely proportional to the square-root of Tu (Fransson et al. 2005), this displacement of the transition region is expected. However, the stabilisation effect is not sufficient to change the transition mechanism since Tu is still superior at 1% in the final state. The presence of streaks, visible on (f), attest to that point. However, a more drastic reduction of Tu, provoked by a more intense shock wave, might result in a change of transition mode.

4.2. *Temporal response of the turbulent boundary layer*

The temporal evolution of the turbulent boundary layer is the purpose of this paper. The change from the old turbulence (initial steady flow) to the new turbulence (which emerges during the transient) is now examined, more specifically. For this investigation, the region of interest is set at $Re_{\theta,i} = 1210$, i.e. at 70% chord. In the following, the shock upstream state is referred with (0) while (1) corresponds to the downstream state.

4.2.1. *Instantaneous flow*

The Figure 9 shows iso-contours of streamwise-velocity fluctuations normalized by the local external velocity $U_e(x,t)$ in a plane parallel to the wall located at $y_0^+ = 5$, in an area close to 70% chord.

The situation (a) corresponds to the initial flow for which many turbulent structures

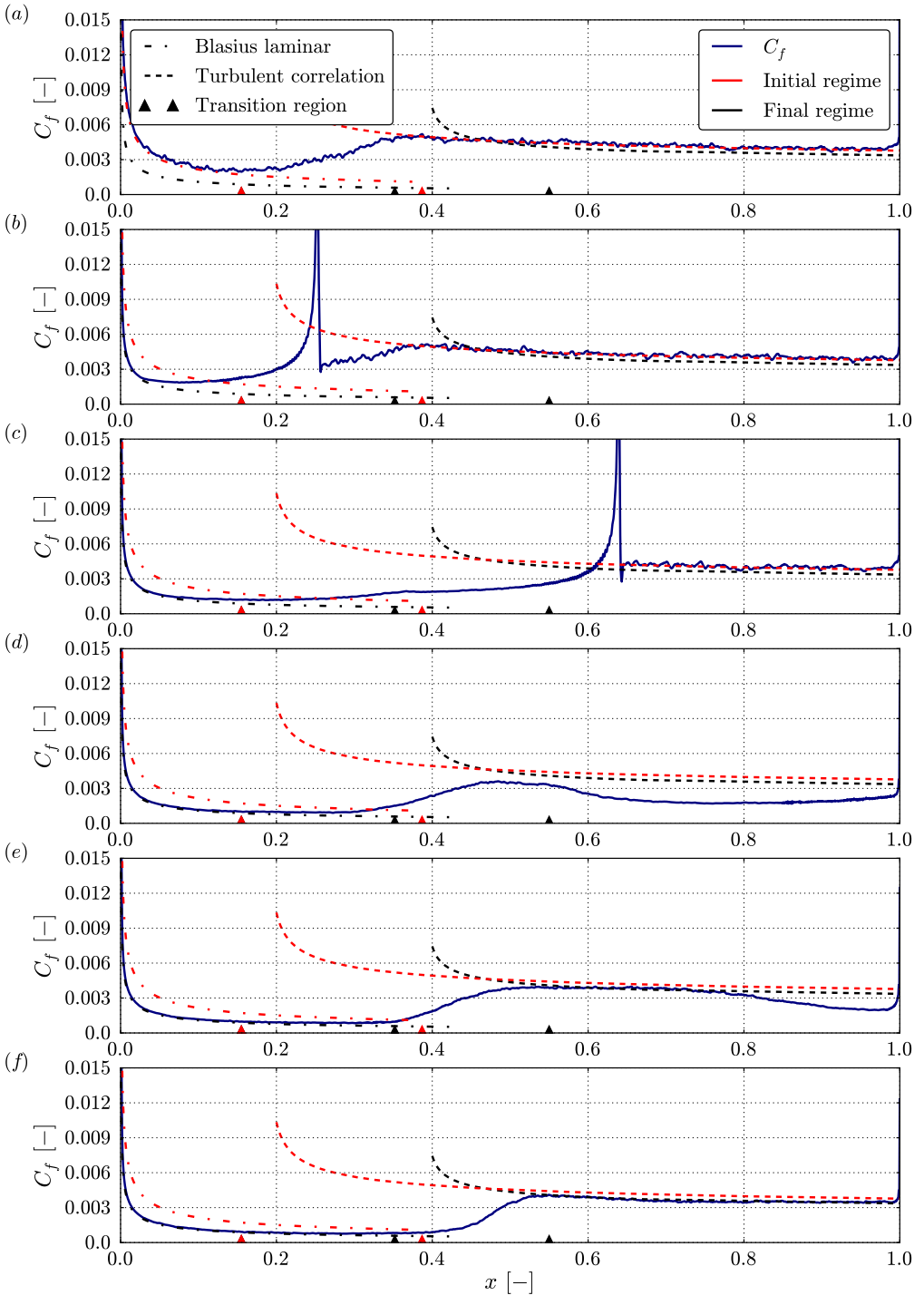

Figure 7: Friction coefficient normalized by local dynamic pressure for several times.

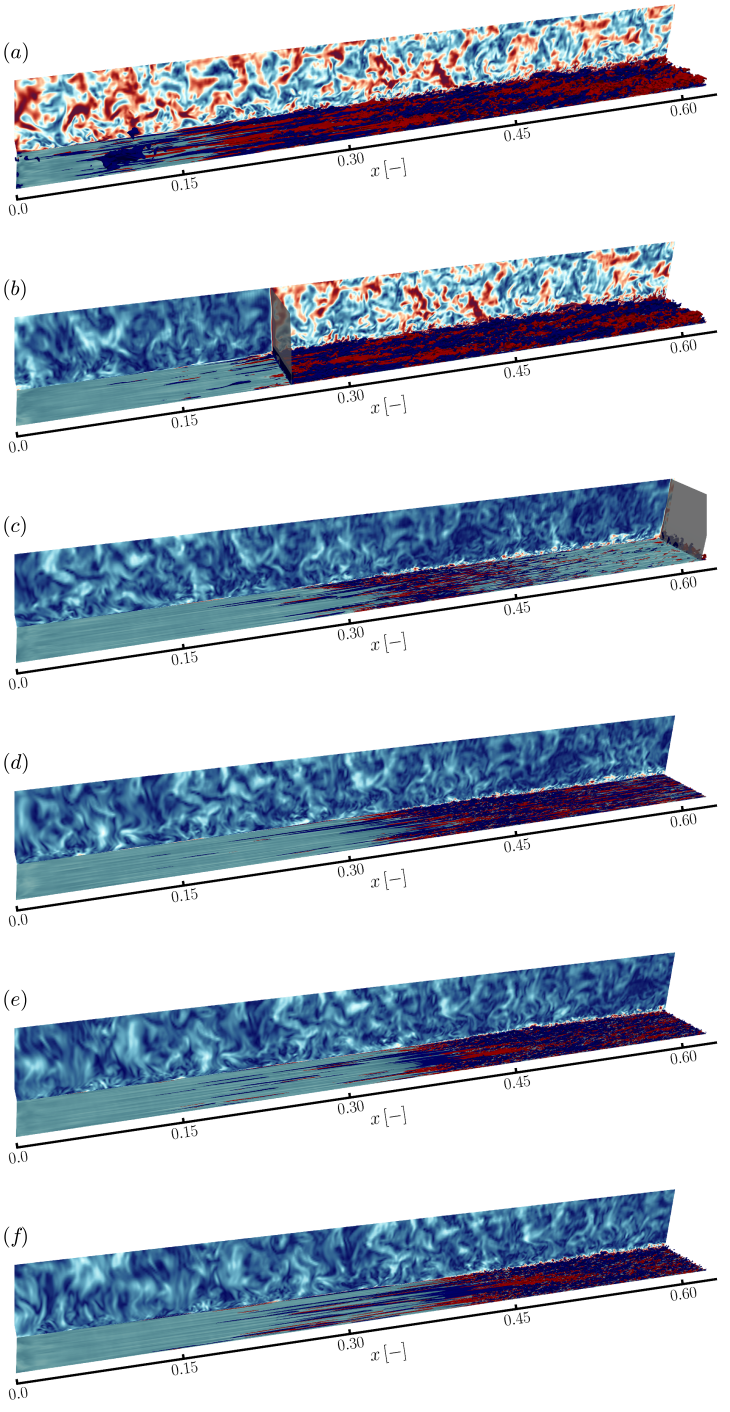

Figure 8: Top: Above the wall: iso-surfaces of high (red) and low (blue) streamwise fluctuating velocity corresponding respectively to $-0.08U_e(x,t)$ and $0.08U_e(x,t)$. Orthogonal to the wall: Free-stream turbulence.

are visible, showing that the boundary layer is *fully turbulent*. In (*b*), the shock is in the analysis region. Immediately behind the shock, the turbulent structures have almost extinguished. Compared with the accelerated velocity of the main flow, the fluctuations are now negligible. Only a few isolated disturbances persist: the flow seems *quasi-laminar*. After a delay, streamwise elongated streaks appear on figure (*c*). Between (*b*) and (*c*), pre-existing turbulent structures are modulated to give rise to streaks. The time needed to observe streamwise streaks after the shock propagation can be interpreted as a *receptivity* process of the boundary layer to pre-existing turbulence. These streaks degenerate to turbulent spots.

The phase between the shock propagation and the first turbulent spots can be named *pre-transition* in relation with the work of He & Seddighi (2013) for an incompressible flow. View (d) reveals the coexistence of turbulent spots with streamwise streaks on the same abscissa: this is the *transition* stage. Turbulent spots get more and more prominent during the transition stage, as illustrated on view (*e*). This stage ends when the turbulence has totally contaminated the boundary layer: it is then *fully turbulent* with the properties of the *new* turbulence, which emerged in (d). The transition from the *old* turbulence to the *new* is therefore not monotonous but follows a temporal transition that has similarities with the spatial bypass boundary layer process. The temporal transition is completed in three stages: *pre-transition*, *transition* and *fully turbulent* boundary layer. These steps exhibit large similarities with the three phases of a bypass spatial process, namely: *buffeted laminar* boundary layer, *transition* and *fully turbulent* boundary layer. Moreover, these steps are very similar to those described by He & Seddighi (2013) observed in incompressible flow. Compressibility does not seem to significantly affect the turbulence dynamic provoked by an acceleration. The analysis of the mean and fluctuating motion which is now proposed helps to confirm this, as well as to reinforce the similarities with the bypass process.

4.2.2. *Mean motion*

The figure 10 shows the temporal evolution of the friction coefficient at 70% of the chord. As observed on the figure 7, a peak of friction follows the shock, which is here located at ($t^* = 0^+$). This peak is provoked by the brutal acceleration of the entire flow, which also generates a thin layer of high strain close to the wall, as we will see below while analyzing the velocity profile. This thin wall shear layer then diffuses into the boundary layer, causing a drop in the friction coefficient. This phase is the *pre-transition* step ($t^* < 8.0$). When the first turbulent spots appear, the friction coefficient begins to increase: this is the beginning of the *transition* phase ($t^* = 8.0$). When the *transition* ends, the friction is constant at the value corresponding to the Re_θ of the final regime ($t^* = 16.0$). The temporal evolution of the friction coefficient reveals strong similarities with the spatial development of the friction coefficient of a boundary layer undergoing a bypass transition.

To go further in comparison with a spatial case, He & Seddighi (2013) propose to investigate the temporal evolution of the boundary layer resulting only from the acceleration (i.e. shock propagation). Consequently, the temporal development of the boundary layer is investigated by examining the differential boundary layer, see equation 4.1, where $U_{b,0}$ ($U_{b,1}$) represents the external flow velocity for the initial (final) flow.

$$\hat{\overline{u}}(y/\delta, t^*) = \frac{\overline{u}(y/\delta, t^*) - \overline{u}(y/\delta, 0)}{U_{b,1} - U_{b,0}} \tag{4.1}$$

The graph on the left side of figure 11 represents the differential velocity profile in the boundary layer as a function of $y/\delta(t)$. Immediately following the wave passage, $\hat{\overline{u}}$ is

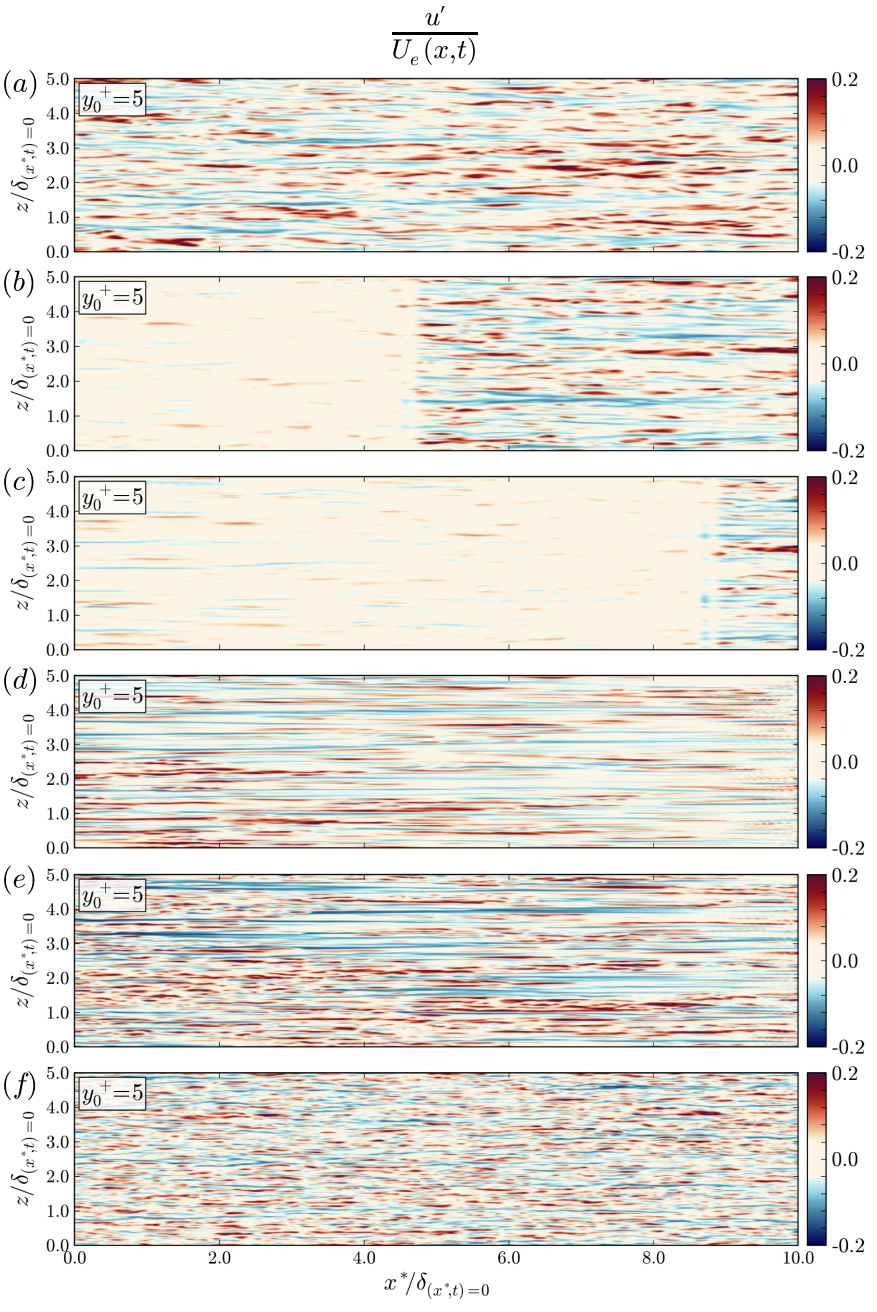

Figure 9: Streamwise fluctuating velocity iso-surfaces normalized by local external velocity $U_e(x,t)$. $x^* = 0$ correspond to 70% of the chord.

close to 1 in almost all the boundary layer except very close to the wall. This means that the acceleration imposed by the shock wave is constant throughout the boundary layer thickness which reacts as a whole, except the very near-wall region. The velocity profile recorded at $t^* = 0.4$ shows how intense is the shear layer. The diffusion of this layer in the core of the boundary layer is the key phenomenon, initiating many mechanisms

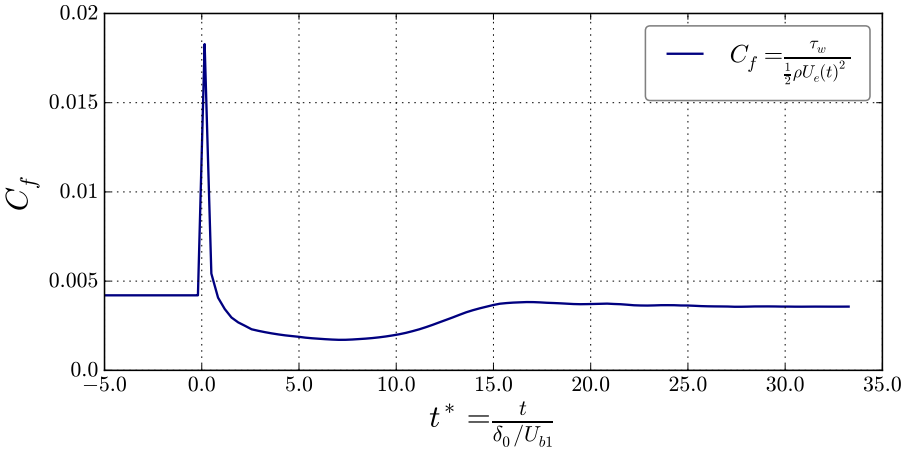

Figure 10: Temporal evolution of the friction coefficient at 70% chord.

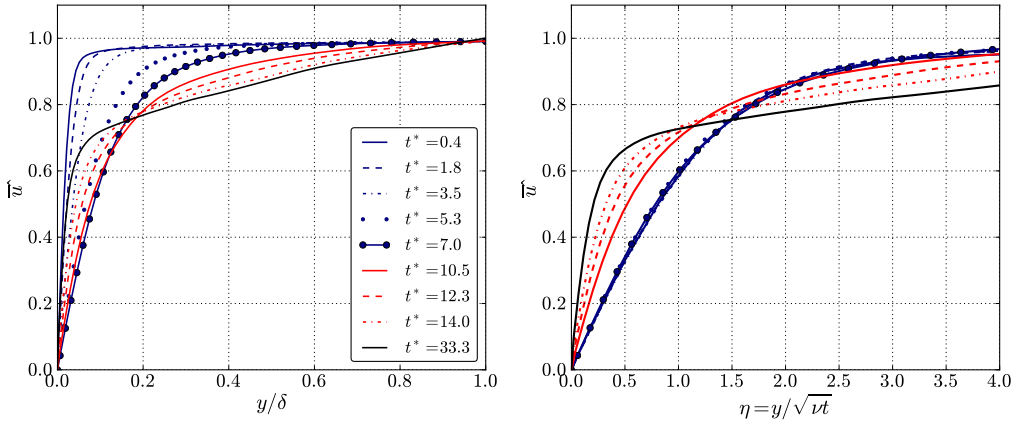

Figure 11: Normalized differential velocity during the transient flow at 70% of chord. Blue: *pre-transition*, red: *transition*, black: *fully turbulent*.

during the transient. This diffusion is very clear during the *pre-transition* phase (between $t^* = 0.4$ and $t^* = 7.0$), while the differential velocity profile in the outer region of the boundary layer remains essentially unchanged. Then, for $t^* > 7.0$, the outer regions of the profile get affected, and the wall shear stress starts increasing: the *transition* phase has begun.

The present *pre-transition* stage looks quite similar to a laminar boundary layer, according to the evolution of the friction coefficient presented above. This is further detailed, and the usual self-similarity of laminar flows are sought, such as the one observed for the normalized velocity profile as a function of the normalized wall distance $\eta = y/\delta(x)$, see Schlichting & Gersten (2017).

However, the differential velocity profiles ($\widetilde{u}$), plotted against $y/\delta(t)$, does not show any self-similarity during this phase. The difficulty comes from the offset introduced by the initial value of the boundary layer thickness. This problem does not exist for conventional spatial analysis of a flat plate boundary layer since the thickness is null at the leading edge. For the present investigation, compensation is required to reveal the

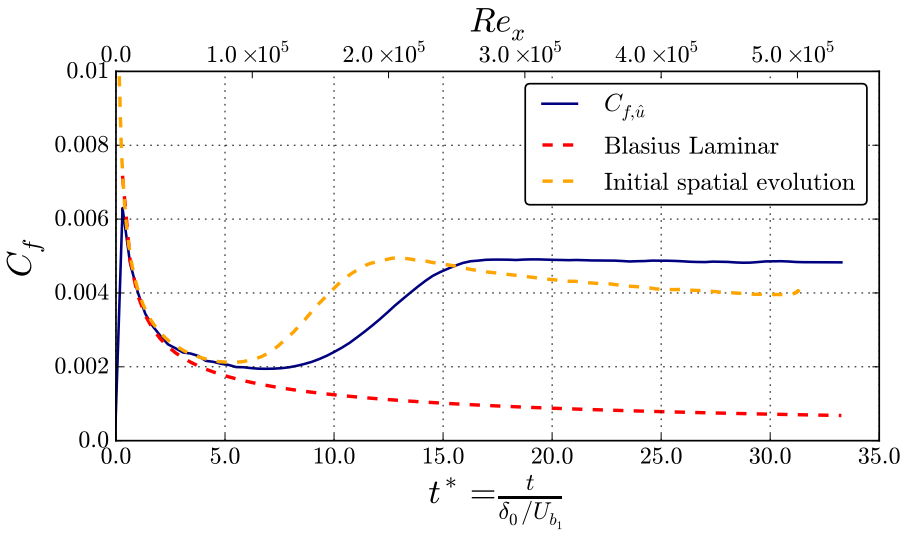

Figure 12: Temporal evolution of friction coefficient based on differential velocity. $C_f = \frac{\tau_{w,\hat{u}}}{1/2\rho U_{b,1}^2}$ with $\tau_{w,\hat{u}} = \mu \frac{\partial[u(y/\delta,t^*) - u(y/\delta,0)]}{\partial y}$.

self-similarity: subtraction of the initial thickness of the boundary layer is performed so that our fictitious thickness is zero before the shock propagation. The velocity profiles are then displayed as a function of $\eta = \frac{y}{\delta(t)-\delta_0} = \frac{y}{\sqrt{\nu t}}$. The figure 11 finally demonstrates that a self-similarity actually exists during the *pre-transition* stage. The temporal development of the differential boundary layer thus follows a laminar-like growth process during the *pre-transition*. This is consistent with the instantaneous flow visualizations. Indeed, downstream of the shock wave, despite some pre-existing residual turbulence, no turbulent spots can be observed until the beginning of the *transition* stage. Only streaks appear during this stage, which is typical of a *buffeted laminar* boundary layer.

A more direct comparison of the two transitional processes, spatial and temporal, is now proposed in figure 12. It is based on the mean flow features trough the friction coefficient. A reference velocity is required to synchronize those two plots, and have a good correspondence between x (or here Re_x) and t^*. This reference velocity is obtained by minimizing the difference between the synchronized temporal friction and the Blasius solution in the quasi-laminar region, which gives a value of $0.76U_{b,1}$. The final correspondence between the two mechanisms is striking. The deviation compared with the Blasius laminar prediction is observed at the same location. This suggests that the receptivity of those two boundary layers is quite similar. In the spatial case, it is a receptivity to external disturbances. In the temporal one, a receptivity to the residual *old* turbulence. The characteristic time of such a receptivity looks comparable in the two cases. Interestingly, the maximum turbulence rate in the initial boundary layer and that of the external flow in the initial spatial case are also comparable. Indeed, the maximum turbulence rate in the initial boundary layer is approximately equal to 5%† to $y_0^+ = 12$, which corresponds to the turbulence rate of the external flow during the initial regime. However, this turbulence is strongly anisotropic in one case, while it has isotropic properties in the other. However, the start of the *transition* phase does not happen at

† When normalized by the external post-shock velocity.

the same time ($t^* = 5.0$ for the spatial case against $t^* = 8.0$ for the temporal case). This is certainly caused by a change in the mechanism at the origin of turbulent spots. Unlike spatial evolution, when the differential boundary layer becomes *fully turbulent*, friction becomes constant. The transient regime then ends in the near-wall region and the flow there reaches an equilibrium corresponding to the characteristics of the *new* turbulence.

4.2.3. *Fluctuating motion*

The response of the fluctuating field, which initiate the different changes in the mean flow, is now detailed. It reinforces the understanding of the different phases of the process which were previously presented.

A representation of Reynolds stresses at 70% of the chord during the establishment transient of the new equilibrium of the boundary layer is given in figure 13. The boundary layer characteristic thicknesses are also reported and the steps of the transitional process recalled. Reynolds stresses are normalized here by the external velocity of the boundary layer and thus reflect the turbulence influence on the mean flow. When the shock crosses the abscissa at $t^* = 0$, the normalized Reynolds stresses experience a sudden drop and reach a very low level which persists all along the phase (0) . The turbulence influences on flow dynamics is weak compared to their contribution to the pre-shock flow ($t^* < 0$). However, a different normalization (figure 15) shows that the absolute level of fluctuations is very comparable to that of the pre-shock situation. The shock wave accelerates the flow but freezes the intensity of fluctuations at its initial level, all along this first phase†. This explains why the flow can be considered as *quasi-laminar* immediately after the wave passage and explains why the differential boundary layer is laminar during this stage. Also, the *receptivity* process of the boundary layer to those pre-existing perturbations is underway, and the phase (1) begins when the streamwise Reynolds stress (u'_{rms}) growth is significant.

Only the streamwise component takes benefits from a production term (see Cebeci & Cousteix (2005)) which explains why it is the first one to respond. But this response is not instantaneous, despite the very intense shear layer created by the wave near the wall. The production term $\left(-\rho\overline{u'v'}\frac{\partial\overline{U}}{\partial y}\right)$ is the product of the normal mean velocity gradient and the turbulent shear stress. The latter is substantially zero near the wall, up to approximately $y_0^+ = 5$. However, pre-existing turbulent structure persists elsewhere in the boundary layer and provides the disturbances on which the *new* turbulence will emerge. So the delay in the response of u'_{rms} is the characteristic time required by the diffusion of the shear layer to reach heights where the turbulent shear stress is no longer negligible. Then the production term is activated and the streamwise elongated streaks form. Stages (0) and (1), cf figure 13, correspond to the *pre-transition* stages according to He & Seddighi (2013). The increase in the growth rate of the production term as the *pre-transition* step is shown in figure 14, where the temporal evolution of the production integrated over the boundary layer thickness is given. During *pre-transition*, the turbulent kinetic energy is therefore essentially concentrated in the streamwise component of the fluctuating motion through streaks. At the end of this step, the turbulence's anisotropy level is, therefore, very high compared to that of an equilibrium turbulent boundary layer.

The *pre-transition* stage ends as soon as the pressure strain term activates the turbulent kinetic energy redistribution through the responses of v'_{rms} and w'_{rms}. These two stresses are thus activated together and indicate the appearance of turbulent spots and the beginning of the *transition* phase. In the present configuration, the *transition* starts for $u'_{rms,max}/U_{b,1} \approx 10\%$. This value is in agreement with the critical amplitude predicted

† There is actually a very slight amplification of u'_{rms} during this phase.

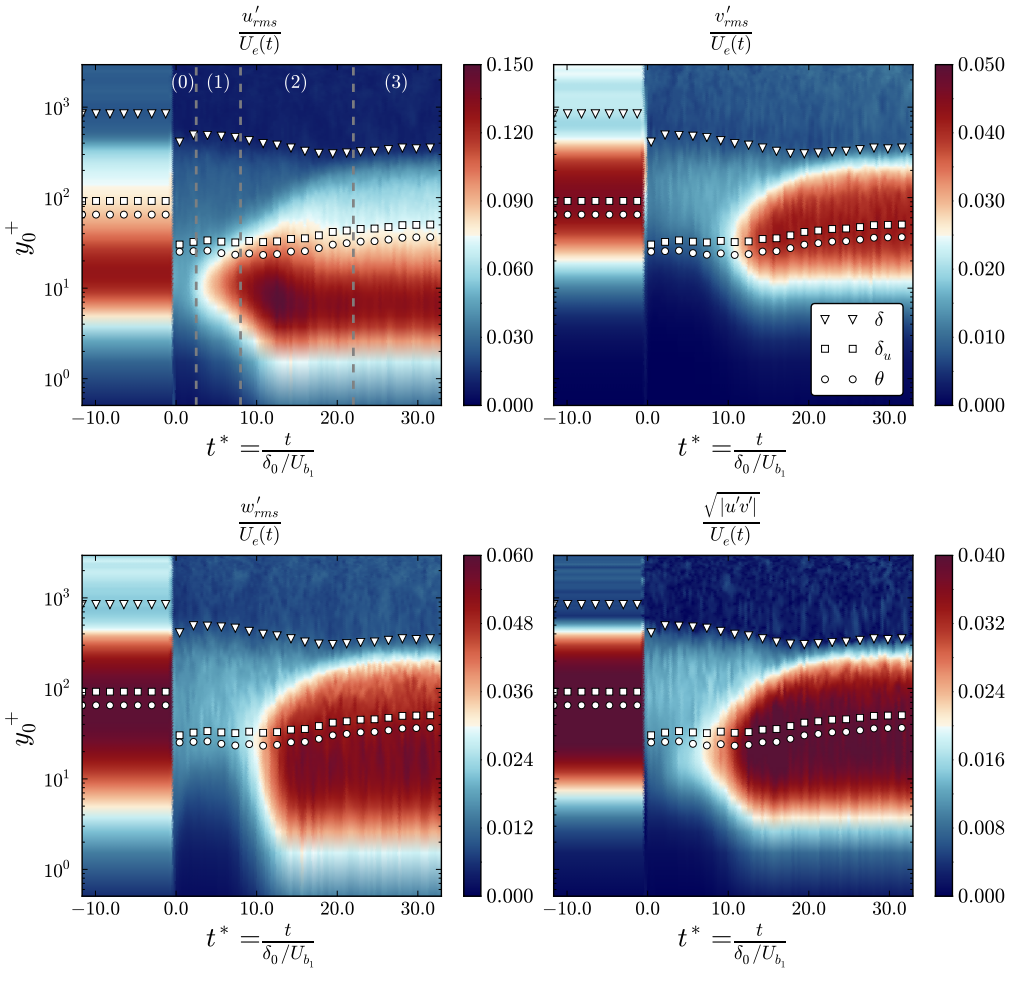

Figure 13: Reynolds stresses normalized by the external velocity ($U_e(x,t)$) during the transient flow. (0): receptivity process, (1): streaks growth, (2): transition and (3): fully turbulent. (0) and (1) correspond to the *pre-transition* stage according to He & Seddighi (2013).

by Vaughan & Zaki (2011) for the streaks, at the beginning of the *transition* stage for a spatial bypass process.

Also, the growth of the maximum of u'_{rms} is observed inside the *transition* stage even though the redistribution term is already active. This is another example of similarities with the usual bypass process: it has been observed in figure 6 while analyzing the spatial transition of the initial boundary layer. The nature of the structures containing the kinetic energy of the fluctuating motion changes continuously during the *transition* stage from elongated streaks to small turbulent spots, resulting in changes in the kinetic energy spectrum during this phase.

At stage (3), the turbulence has contaminated the entire boundary layer thickness. The Reynolds stresses distribution become constant in time: the *transition* phase is over and a steady equilibrium state is found. The boundary layer is thus *fully turbulent*. Some boundary layer regions are fully turbulent before others since the response time differs

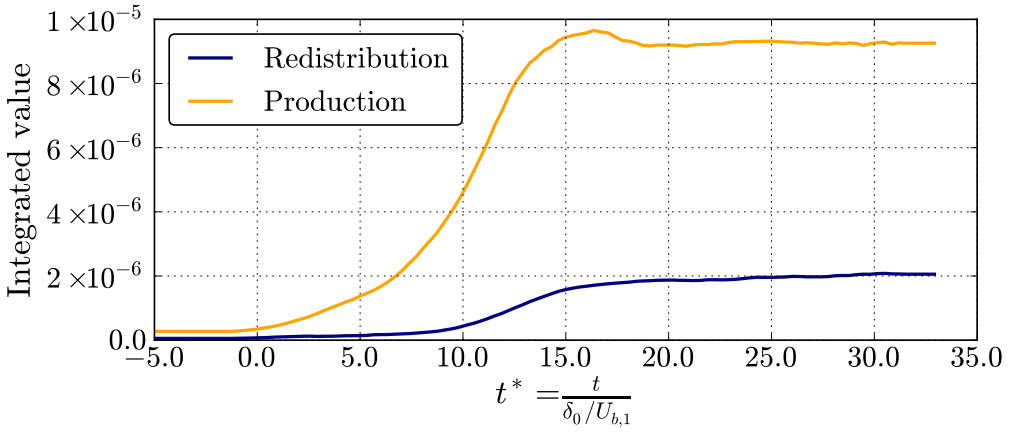

Figure 14: Production and pressure strain terms for u'_{rms} integrated over the boundary layer thickness and normalized by $\rho u_{\tau,0}^4/(\nu\delta_0)$.

from one to another. This is why the transition appears completed at $t^* = 16$ according to the friction coefficient, whereas at this stage, the outer region of the boundary layer is still only slightly affected by the *new* turbulence. In the *fully turbulent* region, the turbulence in the boundary layer thus recovers typical levels of anisotropy.

Finally, let us closely look at the turbulence dynamic behind the wave, which is also identical to that of a bypass spatial transition of the boundary layer. The temporal evolution of maximum turbulent kinetic energy and Reynolds stresses are presented in figure 16. During a bypass transition, the disturbances amplification is linearly related to the longitudinal distance or Re_x. This linearity is also observed in the temporal domain during the *pre-transition* stage, which corresponds to the developments of the streaks ($t^* \in [2.5, 8.0]$). The different delays in the response of Reynolds stresses are particularly evident.

On the same figure 16, the velocity profiles $u'_{rms}/u'_{rms,max}$ are also proposed. During a bypass transition, these velocity profiles present a maximum whose distance to the wall is constant throughout the streak amplification phase, see Luchini (2000). Here the streaks amplification happens when $t^* \in [2.5, 8.0]$. In that time interval, the location of this maximum is recorded constant, approximately at $y/\delta_u = 0.4$. This is closer to the wall than what is generally observed for a spatial bypass process ($y/\delta_u = 1.33$). This difference probably comes from the location at which the perturbations initiating the streaks are found. For the spatial process, it comes from the free-stream turbulence: the outer part of the boundary layer is thus concerned. For the temporal process, it is the residual *old* turbulence which triggers the instability. It is thus present at far more important depths inside the boundary layer. However, the fundamental mechanism remains the same.

5. Conclusions and summary

The boundary layer response to a shock wave propagation was examined on the academic case of the flat plate using large-eddy simulations. The temporal development of the whole spatial boundary layer was first described before focusing on the unsteady evolution of the boundary layer in a region where the boundary layer is turbulent during the initial and final steady flow. It has been shown that the shock wave propagation generates a thin wall shear layer whose temporal development is at the origin of the

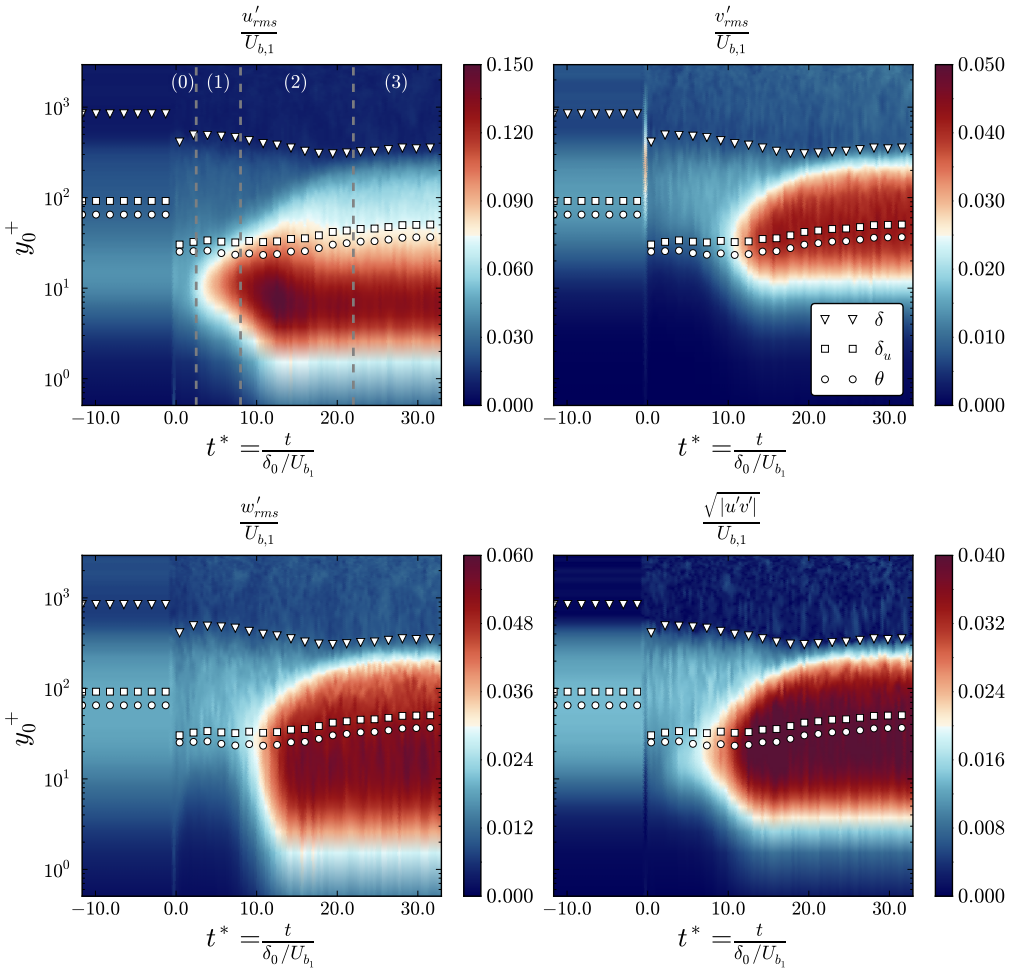

Figure 15: Reynolds stresses normalized by the post-shock external velocity ($U_{b,1}$) during the transient flow. (0): receptivity process, (1): streaks growth, (2): transition and (3): fully turbulent. (0) and (1) correspond to the *pre-transition* stage according to He & Seddighi (2013).

boundary layer changes. The main boundary layer modifications are briefly summarized in chronological order.

Immediately after the shock wave propagation, an intense friction peak is observed, resulting from the interaction between the fluid acceleration in the boundary layer and the no-slip wall boundary condition. The velocity gradient is diffused to the other parts of the boundary layer in the following instants and immediately causes a significant reduction in wall friction. At this stage, the boundary layer appears as *quasi-laminar* and the differential boundary layer exhibits a laminar behaviour, showing an excellent agreement with Blasius theory. This is confirmed by the freezing of the Reynolds stresses during this phase. The turbulence effect on the flow dynamics becomes negligible. However, the turbulent kinetic energy absolute level remains unchanged from its pre-shock level, so that turbulent structures are still present in the boundary layer. This quasi relaminarization

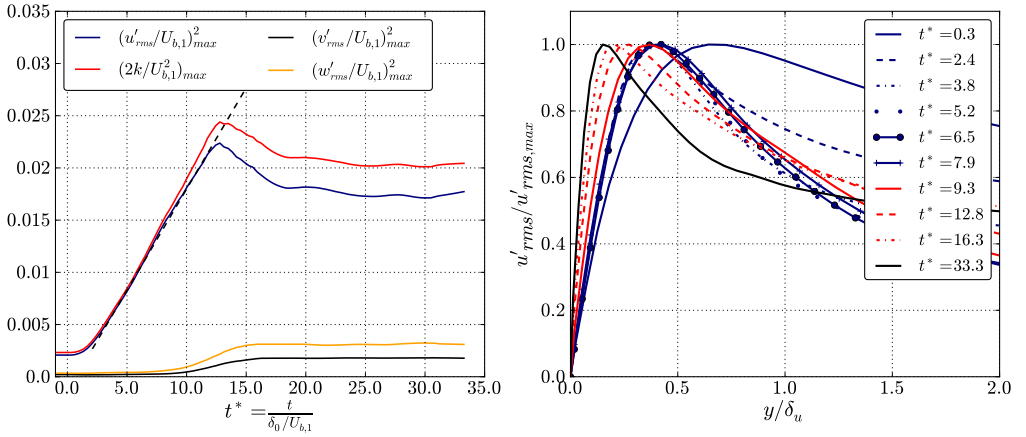

Figure 16: Left: disturbances maximum along the plate. Right: $u'_{rms}/u'_{rms,max}$ profile for several Re_x. $U_{b,0}$ correspond to the boundary layer external velocity of the initial flow.

phase shows strong similarities with the spatial acceleration of a turbulent boundary layer, see for example Launder (1964) or Sreenivasan (1982).

The interaction between the velocity gradient and the pre-existing turbulent structures leads to the production of turbulent kinetic energy. Streamwise elongated streaks are then generated and amplified. The previous phase can thus be interpreted as a *receptivity* process of the boundary layer, toward pre-existing disturbances. This response first occurs close to the wall before diffusing it to the rest of the boundary layer. During this stage, the differential boundary layer begins to deviate from the laminar pattern. The laminar boundary layer is thus *buffeted* in the same way it does for a bypass spatial transition. This step is characterized by a linear disturbance amplification in the boundary layer. During this step, the u'_{rms} profile are scaled by the boundary layer displacement thickness and not by the length scale of the inner region, as it is usually the case for a turbulent boundary layer. These behaviours are shared to a bypass process spatial development. However, it was found that the maximum of u'_{rms} is located closer to the wall compared with a spatial process. This is most likely because the streaks are located, on average, at lower heights in the boundary layer than during a spatial process. Indeed, unlike a transition process induced by free-stream turbulence, the disturbances at the origin of the temporal transition process do not need to penetrate the boundary layer since they are already there.

The *transition* stage starts as soon as the first turbulent spots appear. Spots are generated thanks to the response of the pressure-strain term. This term contributes to taking energy from the streamwise component and redistributing it in the spanwise and normal direction. Streamwise elongated streaks are then destroyed to generate spots. Spots are much more efficient than streaks to promote momentum exchanges between each region of the boundary layer. High velocities are then found close to the wall, which increases the friction coefficient all along the transition. The *transition* ends when the boundary layer thickness is entirely contaminated by turbulence.

When the boundary layer equilibrium is restored along the plate, the boundary layer transition abscissa is shifted downstream from that of the initial steady flow. The stabilizing effect of acceleration on turbulent flow tends to reduce the free-stream turbulence rate, helping to move the transition abscissa away from the leading edge.

It has been demonstrated all along the paper that this temporal transition process

is very similar to a bypass process of a spatial transition. The different stages of the process are dictated by the same energy transfer mechanisms from the mean flow to the fluctuating flow, and then toward fluctuating energy redistribution. The trigger of the transition differs, but this does not affect the process drastically.

This boundary layer temporal transition process is essentially the same as the one depicted by He & Seddighi (2013) during the acceleration of an incompressible flow. It means that the compressible effects have a marginal role in the turbulence dynamics inside the boundary layer after the brutal acceleration induced by the shock.

An interesting perspective would be a generalization of the investigation regarding brutal accelerations: an expansion wave propagating along negative C^- characteristic curves would also create an acceleration, but the boundary layer would be expanded instead of being compressed. Also, the dynamic complexity of turbulence downstream of the wave, due to the time evolution of the anisotropy, is a real challenge for the turbulence models in predicting this kind of flows. The present results constitute an opened database for validation.

Acknowledgements

The authors would like to thank the DGA for their financial support and permitting the research's publication. This work was performed using HPC resources from GENCI-IDRIS and GENCI-CINES on Jean Zay, Occigen (Grant A0082A07178) and CALMIP on Olympe (Grant 2020-p1425).

REFERENCES

Andersson, Paul, Berggren, Martin & Henningson, Dan S. 1999 Optimal disturbances and bypass transition in boundary layers. *Physics of Fluids* **11** (1), 134–150.

Babinsky, Holger & Harvey, John, ed. 2011 Shock wave-boundary-layer interactions. Cambridge ; New York: Cambridge University Press, oCLC: ocn701672464.

Bermejo-Moreno, Iván, Campo, Laura, Larsson, Johan, Bodart, Julien, Helmer, David & Eaton, John K. 2014 Confinement effects in shock wave/turbulent boundary layer interactions through wall-modelled large-eddy simulations. *Journal of Fluid Mechanics* **758**, 5–62.

Brandt, Luca, Schlatter, Phillip & Henningson, Dan S. 2004 Transition in boundary layers subject to free-stream turbulence. *Journal of Fluid Mechanics* **517**, 167–198.

Brès, Guillaume A., Ham, Frank E., Nichols, Joseph W. & Lele, Sanjiva K. 2017 Unstructured large-eddy simulations of supersonic jets. *AIAA Journal* **55** (4), 1164–1184.

Cebeci, Tuncer & Cousteix, Jean 2005 Modeling and computation of boundary-layer flows: laminar, turbulent and transitional boundary layers in incompressible and compressible flows ; with ... 15 tables, 168 problems and a CD-ROM, 2nd edn. Long Beach, Calif: Horizons Publ. [u.a.], oCLC: 180128724.

Fransson, J. H. M., Matsubara, M. & Alfredsson, P. H. 2005 Transition induced by free-stream turbulence. *Journal of Fluid Mechanics* **527**, 1–25.

Hack, M. J. P. & Zaki, T. A. 2014 Streak instabilities in boundary layers beneath free-stream turbulence. *Journal of Fluid Mechanics* **741**, 280–315.

He, S. & Jackson, J. D. 2000 A study of turbulence under conditions of transient flow in a pipe. *Journal of Fluid Mechanics* **408**, 1–38.

He, S. & Seddighi, M. 2013 Turbulence in transient channel flow. *Journal of Fluid Mechanics* **715**, 60–102.

He, S. & Seddighi, M. 2015 Transition of transient channel flow after a change in Reynolds number. *Journal of Fluid Mechanics* **764**, 395–427.

Heiser, William H & Pratt, David T 2002 Thermodynamic cycle analysis of pulse detonation engines. *Journal of Propulsion and Power* **18** (1), 68–76.

Jacobs, Robert G. & Durbin, Paul A. 1998 Shear sheltering and the continuous spectrum of the orr–sommerfeld equation. *Physics of Fluids* **10** (8), 2006–2011.

Jacobs, R. G. & Durbin, P. A. 2001 Simulations of bypass transition. *Journal of Fluid Mechanics* **428**, 185–212.

Jamme, Stéphane, Cazalbou, Jean-Bernard, Torres, Florence & Chassaing, Patrick 2002 Direct numerical simulation of the interaction between a shock wave and various types of isotropic turbulence. *Flow, Turbulence and Combustion* **6** (3), 227–268.

Jung, Seo Yoon & Chung, Yongmann M. 2012 Large-eddy simulation of accelerated turbulent flow in a circular pipe. *International Journal of Heat and Fluid Flow* **33** (1), 1–8.

Jung, Seo Yoon & Kim, Kyoungyoun 2017 Transient behaviors of wall turbulence in temporally accelerating channel flows. *International Journal of Heat and Fluid Flow* **67**, 13–26.

Kendall, J. 1985 Experimental study of disturbances produced in a pre-transitional laminar boundary layer by weak freestream turbulence. AIAA papers.

Klebanoff, P.S 1971 Effect of free-stream turbulence on a laminar boundary layer. Bulletin of the American Physical Society.

Klein, M., Sadiki, A. & Janicka, J. 2003 A digital filter based generation of inflow data for spatially developing direct numerical or large eddy simulations. *Journal of Computational Physics* **186** (2), 652–665.

Landahl, M. T. 1980 A note on an algebraic instability of inviscid parallel shear flows. *Journal of Fluid Mechanics* **98** (02), 243.

Larsson, Johan & Lele, Sanjiva 2009 Direct numerical simulation of canonical shock/turbulence interaction. *Physics of Fluids* **21**.

Launder, B. E. 1964 Laminarization of the Turbulent Boundary Layer in a Severe Acceleration. *Journal of Applied Mechanics* **31** (4), 707–708.

Lee, B.H.K. 2001 Self-sustained shock oscillations on airfoils at transonic speeds. *Progress in Aerospace Sciences* **37** (2), 147–196.

Luchini, Paolo 2000 Reynolds-number-independent instability of the boundary layer over a flat surface: optimal perturbations. *Journal of Fluid Mechanics* **404**, 289–309.

Maruyama, Toshiro, Kuribayashi, Toshisaki & Mizushina, Tokuro 1976 The structure of the turbulence in transient pipe flows. *Journal of Chemical Engineering of Japan* **9** (6), 431–439.

Mathur, A., Gorji, S., He, S., Seddighi, M., Vardy, A. E., O'Donoghue, T. & Pokrajac, D. 2018 Temporal acceleration of a turbulent channel flow. *Journal of Fluid Mechanics* **835**, 471–490.

Matsubara, M. & Alfredsson, P. H. 2001 Disturbance growth in boundary layers subjected to free-stream turbulence. *Journal of Fluid Mechanics* **430**, 149–168.

Mayle, Robert Edward 1991 The role of laminar-turbulent transition in gas turbine engines. *Turbo Expo: Power for Land, Sea, and Air*, vol. Volume 5: Manufacturing Materials and Metallurgy; Ceramics; Structures and Dynamics; Controls, Diagnostics and Instrumentation; Education; IGTI Scholar Award; General.

Reynolds, Osborne 1883 III - an experimental investigation of the circumstances which determine whether the motion of water shall be direct or sinuous, and of the law of resistance in parallel channels. *Proceedings of the Royal Society of London* **35** (224-226), 84–99.

Schlatter, Philipp, Brandt, Luca, de Lange, H. C. & Henningson, Dan S. 2008 On streak breakdown in bypass transition. *Physics of Fluids* **20** (10), 101505.

Schlatter, Phillip & Örlü, Ramis 2010 Assessment of direct numerical simulation data of turbulent boundary layers. *Journal of Fluid Mechanics* **659**, 116–126.

Schlichting, Hermann & Gersten, Klaus 2017 Boundary-Layer Theory.

Sreenivasan, K. R. 1982 Laminarescent, relaminarizing and retransitional flows. *Acta Mechanica* **44** (1-2).

Touber, Emile & Sandham, Neil D. 2009 Large-eddy simulation of low-frequency unsteadiness in a turbulent shock-induced separation bubble. *Theoretical and Computational Fluid Dynamics* **23** (2), 79–107.

Vaughan, Nicholas J. & Zaki, Tamer A. 2011 Stability of zero-pressure-gradient boundary layer distorted by unsteady klebanoff streaks. *Journal of Fluid Mechanics* **681**, 116–153.

Vreman, A. W. 2004 An eddy-viscosity subgrid-scale model for turbulent shear flow: Algebraic theory and applications. *Physics of Fluids* **16** (10), 3670–3681.